Journal of Hydrology 606 (2022) 127438

Contents lists available at ScienceDirect

Journal of Hydrology

journal homepage: www.elsevier.com/locate/jhydrol

Research papers

Simultaneous observations revealed the non-steady state effects of a tropical storm on the export of particles and inorganic nitrogen through a river-estuary continuum

Jingjie Lin [a,b], Michael D. Krom [c,d], Fenfang Wang [a,b], Peng Cheng [b], Qibiao Yu [a,b], Nengwang Chen [a,b,*]

[a] Fujian Provincial Key Laboratory for Coastal Ecology and Environmental Studies, College of the Environment and Ecology, Xiamen University, Xiamen, PR China
[b] State Key Laboratory of Marine Environment Science, Xiamen University, Xiamen, PR China
[c] Morris Kahn Marine Station, Charney School of Marine Sciences, University of Haifa, Haifa, Israel
[d] School of Earth and Environment, University of Leeds, Leeds, UK

ARTICLE INFO

This manuscript was handled by Nandita Basu, Editor-in-Chief, with the assistance of Rebecca Muenich, Associate Editor

Keywords:
Estuarine turbidity maxima
Storm flow
Biogeochemical sediment incubator
Nitrogen cycling
Nitrogen isotope
Jiulong River

ABSTRACT

An important consequence of storms in river-estuary systems is major changes in hydrology and nutrients being fluxed from the land to the coastal ocean. However, the impacts of storms on the nature and amount of dissolved inorganic nitrogen (DIN) in the river-estuary continuum are poorly understood. In this study, two week's continuous observations on two lower riverine fixed stations and an estuarine fixed station in the Jiulong River (SE China) were carried out during a complete storm event in June 10th to 23rd 2019. Suspended particulate matter (SPM), nitrogen species and their isotopic ratios, nitrifying and denitrifying functional genes were measured. The increased river discharge caused the freshwater-brackish water boundary to move downstream and altered the pattern of particle distribution and the location of the estuarine turbidity maximum. The increased river SPM and inorganic nitrogen was associated with watershed soil erosion, sediment scour and land use. Both in the river and estuary, the peak concentration of ammonium arrived faster than nitrate. Apart from river inputs, there was an additional increase of 40 ± 8% of DIN supplied within the tidal river and estuary. The additional DIN mostly came from resuspended sediments and catchment runoff, while increased nitrate also came from soil and ground waters, increased nitrification and decreased denitrification in the estuary. These results suggest that during baseflow conditions the wetlands in the upper estuary acts as a temporary nutrient trap and biogeochemical incubator, while in storms the transformed pollutant N was fluxed from the river-estuary continuum to the adjacent coastal areas.

1. Introduction

Anthropogenic nitrogen is a major pollutant which has increased dramatically as a result of major fertilizer use to enable us to feed the world's increasing population (Galloway et al., 2008; Tilman et al., 2002; Vitousek et al., 1997) with greater than 80 million tons of this extra nitrogen now produced artificially by the Haber process (Liu et al., 2005; Tilman et al., 2002). Much of this excess anthropogenic nitrogen is eventually discharged into rivers and from rivers transported via estuaries to coastal waters causing eutrophication problems (Canfield et al., 2010; Duce et al., 2008; Galloway et al., 2004). The nature of the nitrogen reaching the river system depends on the balance of anthropogenic activities in the catchment. In a mixed activity catchment such as the Jiulong River in S.E. China, an important source of excess nitrogen is from the washout of excess fertilizers applied to the land in the form of ammonia and/or urea fertilizers (Lin et al., 2020a). These fertilizers accumulate in surface soil waters and are subsequently discharged into the river often after having been converted to nitrate by in-situ nitrification processes (Huang et al., 2020; Zhang et al., 2021). The other main source of anthropogenic nitrogen in the Jiulong river system is from human sewage discharges from the population centers and from wastes from intensive animal farming (Bai et al., 2019; Lin et al., 2020b). Once discharged into the river channel microbial and other biological processes can change the nature of the anthropogenic

* Corresponding author at: College of the Environment and Ecology, Xiamen University, Xiamen 361102, PR China.
E-mail address: nwchen@xmu.edu.cn (N. Chen).

https://doi.org/10.1016/j.jhydrol.2022.127438
Received 10 May 2021; Received in revised form 15 November 2021; Accepted 5 January 2022
Available online 10 January 2022

nitrogen by biological uptake, nitrification, denitrification, anammox and other more minor processes both in the river, reservoirs and estuary (Kaushal et al., 2021; Lin et al., 2020a).

While all of these processes occur during normal river flow, the largest fluxes of nitrogen from the catchment to the sea occurs during major storms (Gao et al., 2018; Koschorreck and Darwich, 2003; Rozemeijer et al., 2021). During major storms, there is generally higher soil erosion resulting in higher suspended particulate matter (SPM) in the river channel (Baborowski et al., 2004; Chen et al., 2018b). Excess fertilizers, flushed from the fields, soil waters and groundwater, are discharged into streams and rivers and transported at higher water discharge rates (De Girolamo et al., 2017; Marcé et al., 2018). Storm flow also often causes increased water flow into and through sewage treatment works and intensive agricultural farms (Whitehead et al., 2015). Together these processes result in a pulse of higher nitrogen down the river and through the estuary to the sea.

Estuaries are important locations for biogeochemical processes which can alter nutrient fluxes to the coastal sea. During normal flow, upper estuaries act as traps for nutrients (Sanders et al., 1997). An important component of this trapping is particulate matter with its associated labile particle organic matter (PON) which is deposited (Kaiser et al., 2014), in adjacent creeks and mudflats (Jickells et al., 2016). In sub-tropical estuaries such as the Jiulong River, an important component of such areas is fringing mangrove forests (Yu et al., 2015). Such wetland locations can act as biogeochemical incubators in which diagenetic changes occur in surface sediments which result in changes in chemical nature of the pollutant nitrogen by processes such as ammonification and nitrification and in loss to the atmosphere by denitrification and anammox (Dong et al., 2009; Kessler et al., 2018; Smith et al., 2015). Such processes are particularly important in the surficial sediments of mangrove wetlands (Wang et al., 2019; Wang et al., 2021; Zhang et al., 2020). Recently the wetland areas of estuaries worldwide are being reduced as a result of land reclamation which reduces the ability of estuaries to act as nutrient traps (Jickells et al., 2016) and changes the niche and community of nitrogen cycling microbes (Oczkowski et al., 2020). This general process has also occurred in the Jiulong River estuary (Wang et al., 2018). However, during storms, sediment from these wetlands can be resuspended, releasing the transformed nutrients into the water column and hence fluxed through the estuary to the coast (Chen et al., 2018a; Chen et al., 2018b). An important effect of climate change is that there are more frequent extreme weather events, including larger storms (Annamalai and Liu, 2005; Rozemeijer et al., 2021). These general changes increase the importance of understanding in detail the effects of major storms on anthropogenic nitrogen processes and fluxes into the river catchment and through the estuarine system discharging into the ecologically vulnerable coastal areas.

River watersheds and coast seas were traditionally regarded as two separate systems. We have recognized the importance of adopting a holistic perspective in the studies as well as management of these two systems as a whole body, but simultaneous observations are still limited. In this study we set out to determine in detail the effect of a major storm on the concentration and flux of nitrogen species, to and through the Jiulong river-estuary system in S.E. China. We intensively sampled the river both at the freshwater discharge points from the North and West Jiulong River and at a station in the middle of the estuary, to determine the rate of water discharge, and the concentrations of SPM, the nitrogen species and their isotopic content. The aim was to identify and quantify the fluxes out from the river catchment and estuary during the storm and particularly to examine and understand the biogeochemical and microbial processes which caused increases in the amount and changes in the nature of the nutrients fluxing through the estuary to the coast during the storm. The study particularly shows how transformative processes in the upper estuary sediment incubator changes the nature and flux of N species through the river-estuary system under storm condition.

2. Materials and methods

2.1. Study site

The Jiulong River is the second largest river in Fujian province (Southeast China), which flows into Xiamen Bay and thence to the Taiwan Strait (Fig. 1), with 14,740 km^2 drainage area and 3.5 million population in the river catchment. The multi-year average rainfall in the watershed is 1400–1800 mm (Chen et al., 2018a), which is concentrated between May and August (Fig. 2a). Its subtropical monsoon climate causes high temperature and rainfall in summer, when is frequently buffeted by tropical cyclones and storms. The average daily total river discharge arriving to the estuary from the closest hydrological stations (ZD and PN, Fig. 1) during 2016 to 2019 were 741 (2016 El Niño year), 374, 224 (2018 La Nina year) and 425 $m^3 s^{-1}$, respectively.

The water discharge in baseflow to the Jiulong River Estuary (JRE) is derived mainly from the North River (NJR; 66%) with the West River (WJR) supplying the remaining 34% (Chen et al., 2018a). The upper reaches of the NJR pass through Longyan City and adjacent areas where it receives discharges of domestic and animal waste (Lin et al., 2020a). The downstream flow is regulated by step hydropower stations (Lin et al., 2020a). The upper reaches of the WJR pass through large-scale pomelo orchards and then flows past Zhangzhou City, which discharges treated domestic sewage into the river. During periods of high flow, dikes on both the NJR and WJR are opened to control potential flooding upstream and to generate electricity (Chen et al., 2018a). The characteristics of the JRE in baseflow period is a semi-enclosed macrotidal estuary, with 100 km^2 open water area, 3–16 m depth, 2.7–4 m tidal range, typical semidiurnal tide and 2–3 days of average flushing time (Cao et al., 2005). The southern channel of the JRE contains 90% of the discharge to Xiamen Bay.

Three fixed sampling stations are shown in Fig. 1. The lower river stations (stations ZS and JD) were chosen to be located above the reaches affected by tides and represent the downstream boundaries of WJR and NJR. The estuarine Station E is in the middle channel of the southern JRE, and is the core area of estuarine turbidity maxima (ETM) during baseflow period (Yu et al., 2020; Yu et al., 2019). The catchment areas of WJR and NJR are 4011 km^2 and 9635 km^2, respectively. The tidal reach drainage areas above Station E are 306 km^2.

2.2. Sampling campaign

The monitored storm event was the second major storm in the wet season of June 10^{th} to 23^{rd} 2019 (Fig. 2a). There was a period of increased flood discharge from June 11th to June 18^{th} both in the NJR and WJR (Fig. 2a, b). The daily river total discharge was up to a maximum of 2250 $m^3 s^{-1}$. We divided the storm event into four phases (Initial, Rising, Falling and Ending) according to river total discharge (Fig. 2b). The periods of Initial, Rising, Falling and Ending were from 10^{th} to 11^{th} (2 samples), 11^{th} to 15^{th} (32 samples), 15^{th} to 18^{th} (21 samples) and 18^{th} to 23^{rd} (21 samples) in Station E, respectively. The definition of Baseflow and Flood respectively are the periods when the river discharge is less than and more than 1.2 times of the baseflow, as used in our previous research by an automatic segmentation procedure (BFI (F): Smoothed Minima method) (Chen et al., 2018a; Gao et al., 2018; Yu et al., 2019). According to the definition of flooding, the storm event also can be divided into two major states, Baseflow (Initial and Ending) and Flood (Rising and Falling).

A total of 76 water samples were collected in Station E during the storm, including 10 times periods of intensive observation and sampling including 14 h time-series measurement (11^{th} to 17^{th}, 19^{th}, 21^{st} and 23^{rd}; Fig. 2b). One sample was taken for isotopic nitrate and one sample for isotopic ammonium were collected at Station E each day from June 10 to June 19. The water samples were collected using the 5 L plexiglass samplers at 0.5 m depth, situated several meters away from the estuarine bank to ensure that we were sampling the main estuarine conditions.

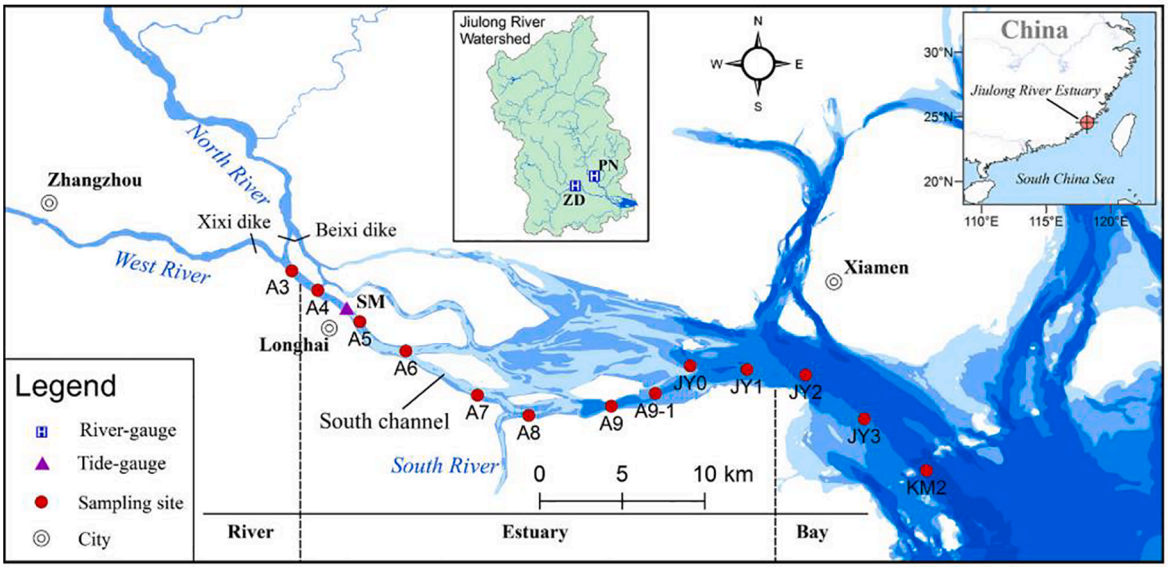

Fig. 1. Map of the Jiulong River Estuary showing the estuary sampling location (E), the tide gauge site at Shima (SM) and the two river gauges in the lower river (ZS and JD). The hydrological stations (ZD and PN) are the closest hydrological stations of sampling location. Light blue indicates shallow water. Red circles are the stations sampled regularly in previous studies (Chen et al., 2018a; Chen et al., 2018b; Yu et al., 2019). (For interpretation of the references to colour in this figure legend, the reader is referred to the web version of this article.)

These water samples were immediately transferred to 1 L brown bottles using the bottom silicone tube on the plexiglass samplers. All samples were immediately placed in portable fridges at 4℃ and then transported to lab every three days to analyze. Immediately before being sampled for analysis, the brown bottles were shaken vigorously. An In-situ multi-parameter sensor (Aqua TROLL 600, USA) was fixed on the bottom water of Station E (1 m above surface sediments) to acquire hourly turbidity and salinity.

A total of 14 water samples were collected in each river station (ZS and JD) per day during these periods of intensive sampling. In Station ZS (WJR), a total of 9 isotopic nitrate samples and 9 isotopic ammonium samples were collected per day. In Station JD (NJR), a total of 8 isotopic nitrate samples were collected per day. The sampling and storage schemes in river stations were the same as for Station E.

2.3. Physicochemical analysis

In the lab, about 500 mL of the water samples were filtered using 47 mm GF/F (0.7 μm) filters. Suspended particulate matter (SPM) was determined as the difference between the unfiltered and filtered GF/F filters after oven-drying (105℃) to constant weight. The filtrate was stored at 4℃ before being analyzed for ammonium (NH_4-N), nitrate (NO_3-N), nitrite (NO_2-N) by segmented flow automated colorimetry (San++ analyzer, Germany) and was determined within less than one week. The precision of nutrient was estimated by repeated determinations of 10% samples with less than 5% relative error. The limit of detection of ammonium, nitrate and nitrite was 0.4 μmol L^{-1}, 0.1 μmol L^{-1} and 0.04 μmol L^{-1}, respectively. Another 50 mL filtrate was stored at −20℃ for subsequent isotopic analysis. The determination of isotopic δ^{15}N-NO_3 and δ^{18}O-NO_3 was carried out by the denitrifier method (Casciotti et al., 2002; Sigman et al., 2001), using Isotope Ratio Mass Spectrometer 100 (IRMS, UK). Isotopic δ^{15}N-NH_4 was determined by ammonia diffusion method (Holmes et al., 1998), using an isotope ratio mass spectrometer (IRMS, Germany).

2.4. Molecular analysis

An additional 1 L of water samples was filtered for analysis of nitrifying and denitrifying functional gene abundances, using the methods given in detail in Lin et al. (2020a). Briefly DNA samples were fileted by 3 μm and 0.22 μm Isopore TM Membrane (47 mm, Millipore, USA) and then stored at −80 ℃. DNA extraction used FastDNATM Spin Kit for Soil (Millipore, USA). The 3 μm and the 0.22 μm filters were used for collecting particle-attached (PA) and free-living (FL) microbes, respectively. Nitrification microbes include ammonia-oxidizing archaea (AOA) and bacteria (AOB) by *amo*A gene and nitrite-oxidizing bacteria (NOB) by *nxr*A gene (Table S1). Denitrification reduces nitrate and nitrite by *nar*G (nitrate reductase) and *nir*S (nitrite reduce). The primers of *amo*A (AOA), *amo*A (AOB), *nxr*A, *nar*G and *nir*S came from Francis et al. (2005), Rotthauwe et al. (1997), Wertz et al. (2008), López-Gutiérrez et al. (2004) and Jung et al. (2011), respectively (Table S1). The qPCR amplification used a Bio-Rad CFX96 qPCR (Table S2).

2.5. Auxiliary data, calculations carried out and statistical analysis

Hourly river discharge was obtained from local government at the closest hydrological stations (ZD and PN, Fig. 1). The tidal range at Shima tide-gauge was obtained from the National Maritime Information Service (https://www.cnss.com.cn/tide/).

The river fluxes were calculated using the formula $\text{Flux}_{\text{NJR/WJR}} = \text{Concentration}_{\text{NJR/WJR}} \times \text{Discharge}_{\text{NJR/WJR}}$ respectively, where the concentration was the measured daily concentration and the discharge was the river discharge at the river exit points. The estuarine flux was calculated using the formula $\text{Flux}_{\text{JRE}} = \text{Concentration}_{\text{low tide}} \times (\text{Discharge}_{\text{NJR}} \times 1.03 + \text{Discharge}_{\text{WJR}} \times 1.08)$, where the concentration was the measured concentrations at low tide (0 PSU) multiplied by the summed daily river discharge modified using the ratios of catchment area, which was 1.03 (NJR) and 1.08 (WJR) between hydrological stations (ZD and PN) and Station E. To identify the impact of the storm events on estuarine velocity and salinity, a three-dimension numerical model (Regional Ocean Modeling System, ROMS), which has been developed for the JRE (Cheng et al., 2019; Cheng et al., 2020). This model calculates salinity and velocity with 15 layers (0.3 m depth per layers), using 48–800 m grid spacing and 339 × 165 grid points. The river discharge conditions used in the model was the measured river discharge during the storm and the average discharge of Baseflow (745 m^3 s^{-1}). The Δ water velocity shown in Fig. 2d indicates the difference between modeled hourly estuarine velocities under the storm and

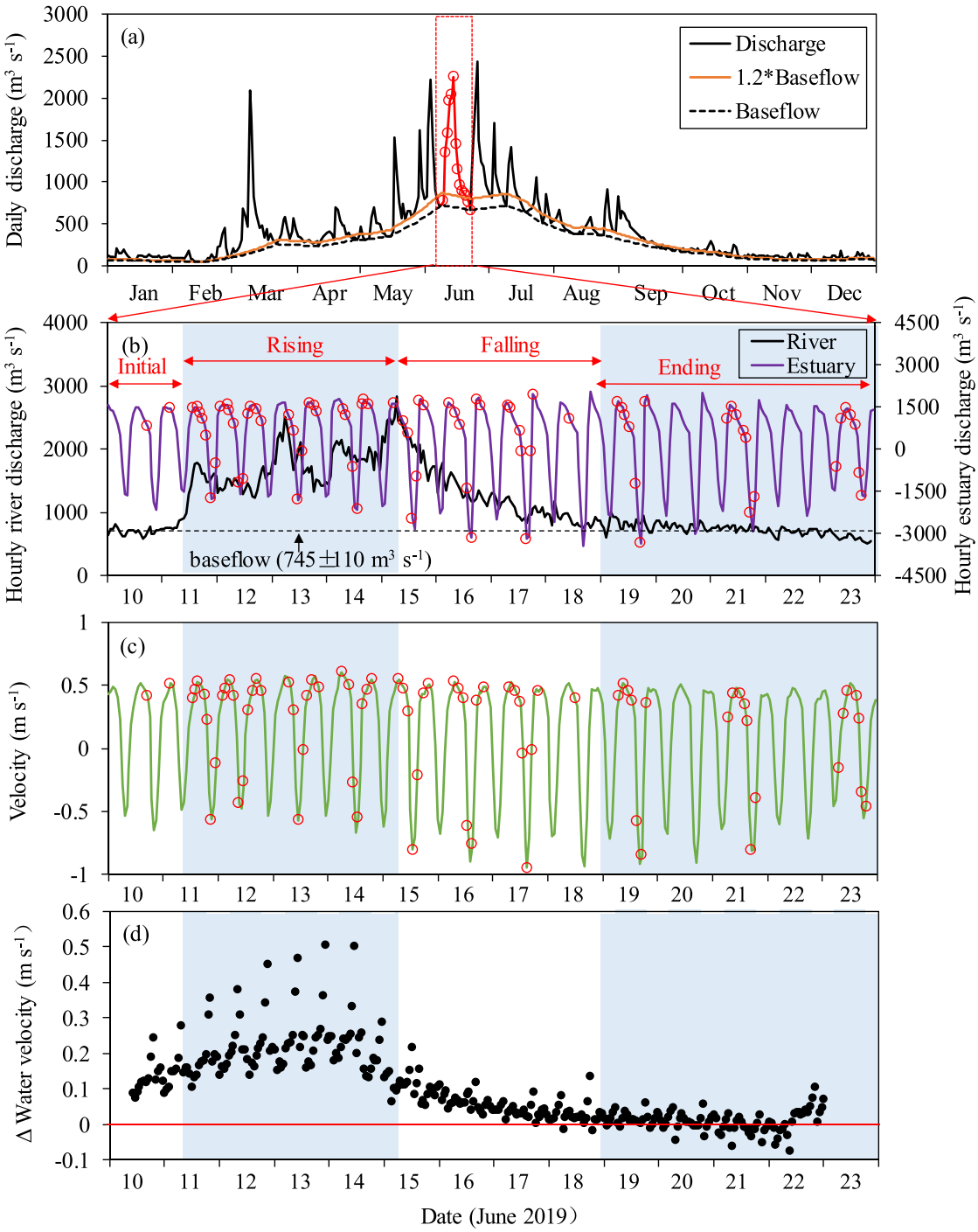

Fig. 2. Hydrography of the river discharge: (a) shows the total discharge through all of 2019 including the peaks and estimated baseflow, (b) shows the hourly total river discharge and estuary discharge during the period of the storm and the tidal changes. The sampling events are shown as red circles, (c) shows the water velocity simulated by daily river discharge at Station E in the Jiulong River Estuary during the period of intensive sampling (sampling events are shown as red circles). Positive values of estuary discharge and velocity were periods during the ebb tide, while negative values were during the flood tide when the net flow was landward. (d) shows the difference (Δ) of simulated water velocity between with and without the effects of the storm. (For interpretation of the references to colour in this figure legend, the reader is referred to the web version of this article.)

Baseflow conditions. Δ Concentration/Flux indicate the difference between the estuary (Station E) and the flow-weighted mean river concentration/summed flux (Stations ZS and JD).

ANOVA analysis was performed using the SPSS program to test the difference of hydrological parameters and N species at low/high tides during the four phases of the storm, using the Kolmogorov-Smirnov test and variances homogeneous test.

3. Results

3.1. Hydrological conditions

During the storm, the NJR contributed 73% ± 4% of the total river discharge to JRE, while the WJR discharge was the remainder. The average hourly river total discharge was 730 ± 88 $m^3 s^{-1}$ in the Baseflow increasing to 1544 ± 442 $m^3 s^{-1}$ in the Flood (Table 1). The hourly

Table 1
Hydrology, particles, nitrogen species concentrations and fluxes (mean ± SD) at Station E during the storm event.

Parameter (unit)	The storm event (June 10th to 23rd 2019)			
	Initial	Rising	Falling	Ending
Total river discharge ($m^3 s^{-1}$)	699.1 ± 53.6^c	1679.2 ± 410.8^a	1360.9 ± 443.7^b	737.0 ± 96.3^c
Seaward discharge ($m^3 s^{-1}$)	966.0 ± 343.6^c	1282.1 ± 377.0^a	1209.3 ± 449.8^b	637.4 ± 199.1^c
Landward discharge ($m^3 s^{-1}$)	1323.1 ± 572.5^b	1184.5 ± 615.2^b	1745.6 ± 988.5^a	688.2 ± 27.5^c
Seaward velocity ($m s^{-1}$)	0.39 ± 0.1^c	0.43 ± 0.12^a	0.41 ± 0.11^b	0.38 ± 0.11^c
Landward velocity ($m^3 s^{-1}$)	0.41 ± 0.18^b	0.35 ± 0.18^c	0.52 ± 0.28^a	0.48 ± 0.25^b
SPM (mg L^{-1})	129.5 ± 59.4^b	187.5 ± 112.5^a	171.8 ± 57.2^a	129.9 ± 57.1^b
DIN (μmol L^{-1})	216.6 ± 5.4^c	265.3 ± 10.6^a	242.8 ± 15.6^b	207.9 ± 9.4^c
NH_4-N (μmol L^{-1})	22.6 ± 1.4^b	36.1 ± 15.8^a	24.2 ± 6.8^b	20.8 ± 5.1^b
NO_3-N (μmol L^{-1})	182.5 ± 6.2^b	210.0 ± 39.0^b	225.1 ± 23.5^a	177.0 ± 12.6^c
NO_2-N (μmol L^{-1})	7.7 ± 1.2^c	8.2 ± 1.0^b	7.2 ± 0.6^c	8.6 ± 3.0^a
NH_4-N/DIN (%)	11.4 ± 1.1^b	13.5 ± 2.8^a	9.7 ± 1.5^b	10.2 ± 1.3^b
NO_3-N/DIN (%)	85.0 ± 1.0^a	83.5 ± 3.1^b	87.3 ± 1.7^a	85.8 ± 0.9^a
ΔSPM (mg L^{-1})	75.8 ± 23.3	123.0 ± 19.4	118.6 ± 53.3	102.3 ± 23.3
ΔDIN (mg L^{-1})	57.3 ± 16.9^b	93.6 ± 16^a	65.6 ± 8.9^b	38.1 ± 23.6^b
ΔNH_4-N (μmol L^{-1})	12.8 ± 0.5^b	18.8 ± 6.5^a	9.8 ± 1.3^b	7.3 ± 2.6^b
ΔNO_3-N (μmol L^{-1})	40.3 ± 16.6^b	72.0 ± 9.7^a	52.4 ± 9.8^b	25.7 ± 20.8^b
ΔNO_2-N (μmol L^{-1})	4.2 ± 0.2	2.8 ± 0.7	3.5 ± 0.6	5.2 ± 1.6
SPM (t d^{-1})	10497.0 ± 908.7^b	37408.0 ± 9769.7^a	16879.8 ± 2092.0^b	12769.7 ± 3301.3^b
DIN (t d^{-1})	419.9 ± 113.6^b	685.7 ± 122.9^a	296.4 ± 58.7^c	222.8 ± 62.5^c
NH_4-N (t d^{-1})	43.1 ± 12.8^b	92.7 ± 35.0^a	28.9 ± 2.1^b	22.7 ± 9.6^b
NO_3-N (t d^{-1})	363.5 ± 97.4^b	575.3 ± 111.7^a	259.3 ± 55.7^b	191.9 ± 51.4^c
NO_2-N (t d^{-1})	13.2 ± 3.5^b	17.7 ± 4.8^a	8.2 ± 1.0^b	8.1 ± 4.2^b
ΔSPM (t d^{-1})	7000.9 ± 291.4^b	24568.8 ± 5386.8^a	11829.3 ± 3383^b	10762.3 ± 2928.3^b
ΔDIN (t d^{-1})	158.2 ± 103.1^b	314.8 ± 69.7^a	94.5 ± 25.1^b	56.4 ± 43.7^b
ΔNH_4-N (t d^{-1})	23.3 ± 6.5^a	55.9 ± 33.4^a	13.5 ± 1.1^b	9.4 ± 8.9^b
ΔNO_3-N (t d^{-1})	127.6 ± 94.4^b	252.8 ± 59.9^a	77.1 ± 24.0^b	42.1 ± 35.6^b
ΔNO_2-N (t d^{-1})	7.4 ± 2.3	6.2 ± 3.6	4.0 ± 0.1	4.9 ± 3.8

Note: The data of discharge and velocity is hourly data. a, b, c and d represent significant differences ($p < 0.05$) among the four phases of the storm event (Initial, Rising, Falling and Ending). The Δ Concentration/Flux shows the difference between the estuary site (E) and the summed river concentration/flux.

estuary discharge and velocity at Station E respectively were 330 ± 1388 $m^3 s^{-1}$ and 0.12 ± 0.44 m s^{-1}. The Δ water velocity, i.e. the increase caused by the storm, was significantly higher during the Rising (0.21 ± 0. 08 m s^{-1}) than the other periods (Fig. 2d).

During the Baseflow, Station E had low salinity (0–3 PSU) at high tide and freshwater at low tide. As the discharge increased (Rising and initial part of the Falling), freshwater occupied Station E. As the discharge decreased (Falling to Ending), there was again increased salinity during periods of high tide at Station E (Fig. 3a, b).

3.2. Variation of suspended particulate matter (SPM)

The average concentration of SPM discharged from the two rivers during the Baseflow was 17 ± 8 mg L^{-1} (WJR) and 32 ± 1 mg L^{-1} (NJR) contributing to the total SPM measured in the JRE of 105 ± 25 mg L^{-1} (Fig. 4a). These concentrations resulted in a calculated riverine SPM flux of 5049 ± 4701 t d^{-1} (NJR) and 918 ± 645 t d^{-1} (WJR) to the JRE, which represented in total 27% ± 10% of the flux calculated as passing through the estuary (20365 ± 12469 t d^{-1}; Fig. 5a).

The SPM discharged from the two rivers increased reaching a peak of 92 mg L^{-1} and 17839 t d^{-1} (total calculated concentration) towards the end of Rising (Fig. 3c). The average concentration and flux of SPM from the river then decreased back to Baseflow values of 27 ± 6 mg L^{-1} and 2007 ± 438 t d^{-1} by the Ending period. During the storm period, in addition to SPM from the rivers, there was additional SPM present in the water column at Station E (Fig. 4a). The flux and Δ flux of SPM at Station E were considerably higher during the Rising than during the other periods (Table 1). In addition to these major average changes in SPM, there were also relatively minor changes in the concentration of SPM at Station E between low tide and high tide (Fig. 1a). The concentration of SPM in surface water was significantly correlated with water velocity during the Baseflow, both in ebb tide and flood tide (Fig. S2a), while the turbidity in bottom water was positively correlated water velocity during the storm, only in flood tide (Fig. S2b).

3.3. Changes in nitrogen species

Both the WJR and NJR contributed riverine nitrogen input to estuary. The WJR had higher concentrations of NH_4-N, NO_3-N, and NO_2-N than NJR (Fig. 4), which resulted in similar total fluxes to the JRE (Fig. 5). Riverine NH_4-N and NO_2-N increased in concentration during the Rising and peaked in the middle of Rising, before the maximum discharge. Then they decreased to a minimum at the beginning of Falling, and returned to baseflow values during the Ending. By contrast, the concentration of NO_3-N in both the NJR and WJR, decreased as the discharge increased during the beginning of Rising and then increased getting close to baseflow concentrations by the beginning of Falling. The storm event changed riverine nitrogen fluxes with different patterns for the NJR and WJR (Fig. 5). All nitrogen species increased fluxes with rising discharge and gradually recovered to Baseflow conditions from the last day of the Rising. Higher fluxes of NH_4-N and NO_3-N were measured in the NJR during the Baseflow, while the fluxes in the WJR exceeded NJR during the Flood.

The patterns of nitrogen concentration and flux observed in the estuary were different from the rivers (Fig. 4, Fig. 5). Estuarine NH_4-N and NO_2-N reached its maximum concentration and flux at the beginning of the Rising, while another peak value of NO_2-N was detected during the Ending (Fig. 6). The ratio of NH_4-N/DIN increased from 11.4% to 13.5% during the Rising (Table 1). By contrast, the concentration and flux of NO_3-N started to rise at the beginning of Rising and continued to increase reaching a maximum at the end of Rising (Fig. 5, Fig. 6). Both the Δ concentrations and fluxes of NH_4-N and NO_3-N were considerably higher during the Rising, while NO_2-N remained roughly similar (Table 1). Comparing the concentration between low tide and high tide, low tide had higher NH_4-N and lower NO_2-N, without any significant difference of NO_3-N (Fig. S1).

3.4. Nitrate and ammonium isotopes

The riverine and estuarine nitrate and ammonium isotopic values are shown in Fig. 7. The ratios of δ^{15}N-NO_3 at Station E (7.0‰ ± 1.6‰) were lower than the samples from the exits from the rivers (7.6‰ ± 0.9‰ WJR and 8.5‰ ± 2.1‰ NJR), except on June 17th. The NJR diluted δ^{15}N-NO_3 to 7.2‰ during the Initial and then increased to 9.2‰ during the Rising, which then gradually decreased with decreasing discharge. The WJR decreased δ^{15}N-NO_3 from 8.2‰ (Initial) to 6.0‰ (Rising) and then increased to 8.1‰ (Falling). By contrast, δ^{15}N-NH_4, estuarine values were lower than the WJR during the Initial and then surpassed it during the Rising until the late Falling. The relationship between δ^{15}N-

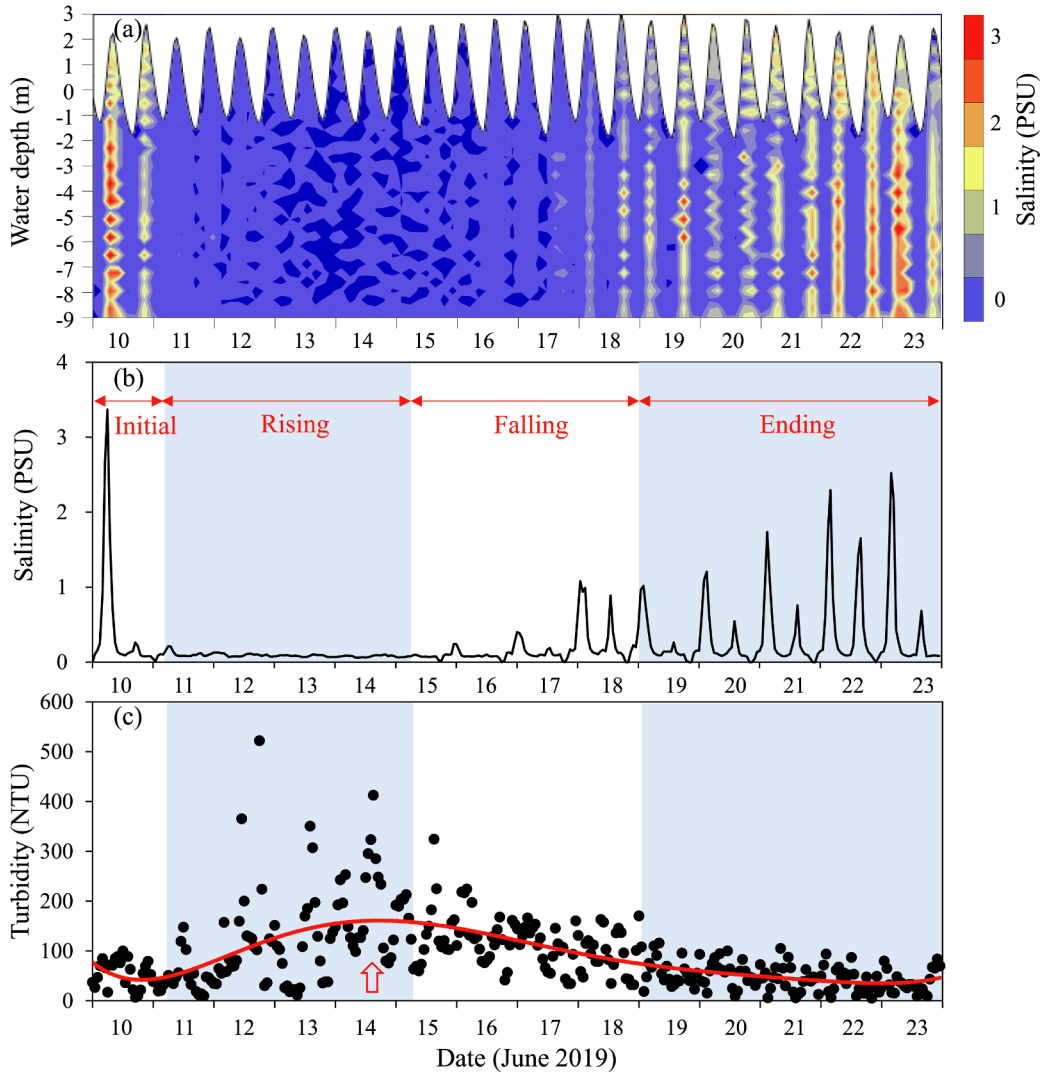

Fig. 3. (a) shows the modelled hourly salinity profile of at Station E over the entire water column during the storm. (b) shows the measured hourly salinity at the bottom depth (1 m above the sediment). (c) shows the hourly turbidity from a meter located 1 m from the bottom in NTU units. The red line is the polynominal fitting curve of the turbidity data. (For interpretation of the references to colour in this figure legend, the reader is referred to the web version of this article.)

NH_4 and daily total river discharge was negative in the WJR but positive in the JRE (Fig. 7d).

3.5. Abundances of nitrogen functional genes

The abundances of nitrifying and denitrifying genes at Station E changed during the storm (Fig. 8). Nitrifying genes *amo*A (AOA), *amo*A (AOB) and *nxr*A (NOB) increased 1.7, 2.6 and 2.1 times during the Flood. The *amo*A (AOA) and *nxr*A genes initially decreased during the first day of Falling and then returned to Baseflow values at the end of Falling, while *amo*A (AOB) remained at peak abundance in the middle of Falling and then decreased during the Ending. For those genes associated with nitrifiers, AOA and NOB reached their maximum abundance faster than AOB. NOB was always less than AOA and AOB during the Baseflow, while it exceeded ammonia-oxidizing microbes (AOA and AOB) during the Flood. AOB was always more than AOA. AOB peaked during the Falling.

By contrast, denitrifying genes *nar*G and *nir*S decreased 2.1 and 1.9 times during peak discharge (Fig. 8d, e). The difference between *nar*G and *nir*S abundances was similar during the Initial and increased with increasing discharge, resulting in far less *nar*G than *nir*S. The *nir*S gene reached low abundance earlier than the *nar*G gene.

4. Discussion

4.1. Effects of the storm on estuarine hydrological and sedimentological conditions

During normal baseflow the freshwater-brackish water boundary is in the region of A5-A7 (Fig. 1), upstream of Station E (Chen et al., 2018b; Yu et al., 2020). This is the location of the ETM zone. During storm flow, the freshwater-brackish water boundary moves downstream depending on the intensity of storms and the corresponding increase in freshwater discharge (Chen et al., 2018a). This was also the pattern in this study (Fig. 3). During the Baseflow, there was fluctuating salinity at Station E changing from 0‰ to 3‰, which is the characteristic of the ETM (Fig. 3a, b). During the Rising and the most of Falling, the water column at Station E was entirely fresh. Therefore, the flow changed to the higher flow rate characteristic of typical river storm flow during the storm (Fig. 3a, b). Once the discharge decreased at the end of Falling and through the Ending period, the freshwater-brackish boundary migrated upstream to mid-estuary (Station E) again, which had tidal changes in salinity again.

These changes in estuarine circulation have important consequences on sediment dynamics. Under normal baseflow conditions, sediments brought down the river together are deposited in the upper estuary

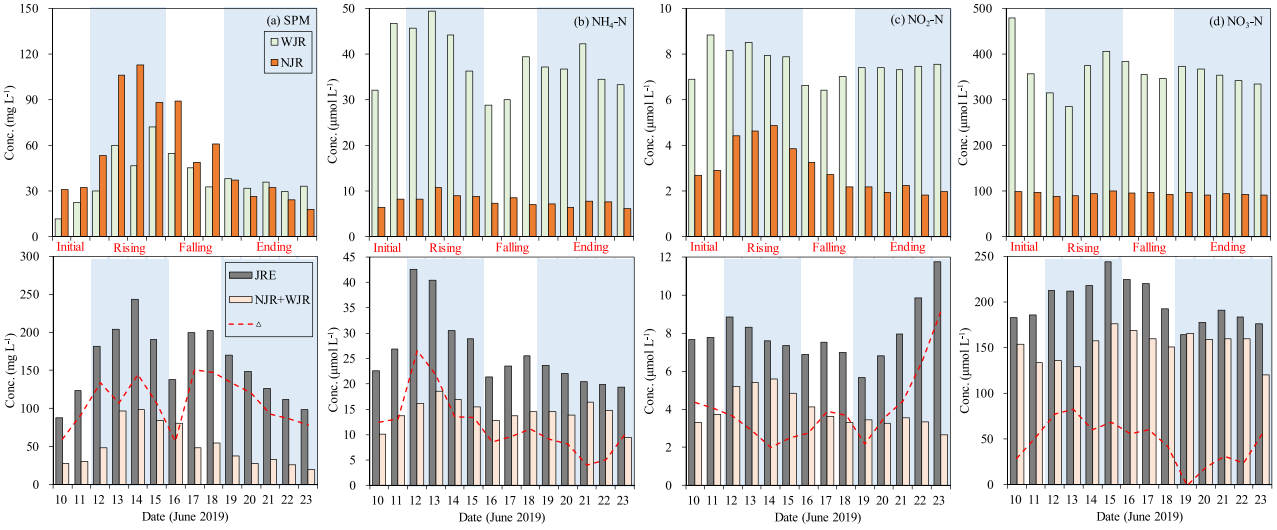

Fig. 4. Temporal concentrations of (a) SPM, (b) ammonium, (c) nitrite and (d) nitrate in the lower river sites (ZS and JD) in the upper diagrams and comparison between the estuary site (E) and the summed river concentrations in the lower diagrams during the storm. The Δ Concentration, shown as a dashed line shows the difference between the estuary site (E) and the summed river concentration.

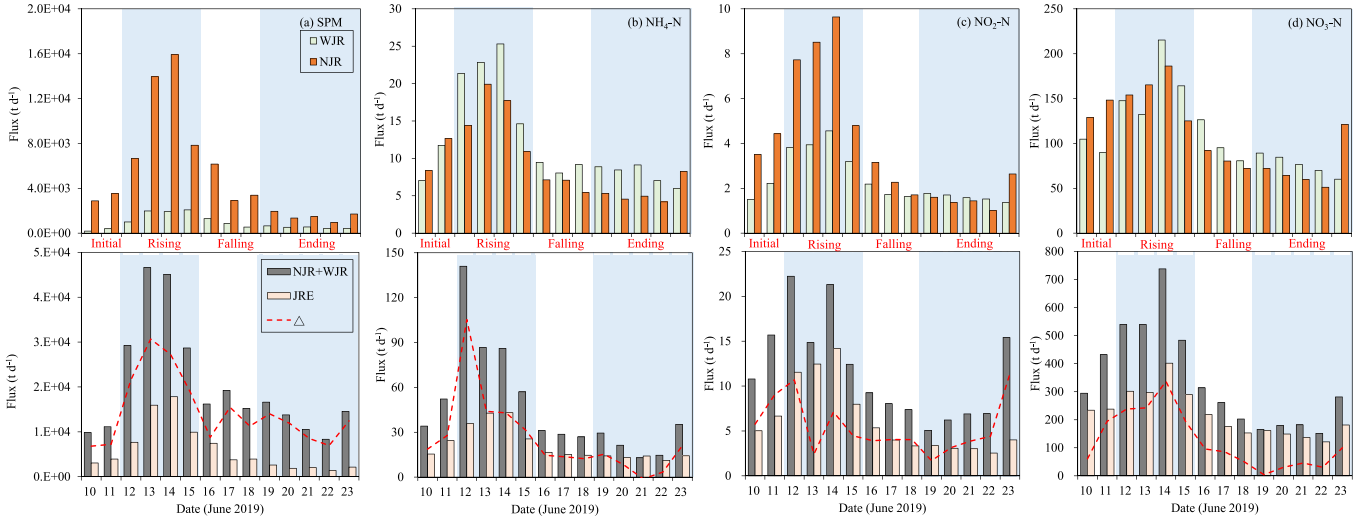

Fig. 5. Temporal fluxes of (a) SPM, (b) ammonium, (c) nitrite and (d) nitrate in the lower river sites (ZS and JD) in the upper diagrams and comparison the addition between the estuary site (E) and the summed river fluxes in the lower diagrams during the storm. The river fluxes were calculated using the formula $\text{Flux}_{NJR/WJR} = \text{Concentration}_{NJR/WJR} \times \text{Discharge}_{NJR/WJR}$ respectively. The estuarine flux was calculated using the formula $\text{Flux}_{JRE} = \text{Concentration}_{\text{low tide}} \times (\text{Discharge}_{NJR} \times 1.03 + \text{Discharge}_{WJR} \times 1.08)$. The ratios of catchment area were 1.03 (NJR) and 1.08 (WJR) between hydrological stations (ZD and PN) and the E site. The Δ Flux shows the difference between the estuary site (E) and the summed river flux.

(above Station E) forming a layer of relatively unconsolidated sediments in the main channel and in the adjacent wetland and side creeks including mangrove wetlands (Chen et al., 2018a; Yu et al., 2020). As typically occurs in storms, there was an increase in total SPM at Station E, which correlated with the increase in freshwater discharge during the Rising (Table 1). This increased SPM was due both to an increase in sediments brought down the river, and an additional increase of SPM due to sediment supplied by local resuspension processes in the upper estuary (Fig. 4a). During rainstorms, the sediments load out from the Jiulong River watershed increases (Chen et al., 2018b). This increase is caused by soil erosion in both the WJR and NJR catchments together with deliberate flushing of sediments behind some of the hydroelectric dams, particularly in the NJR (Chen et al., 2018a).

In addition, there are also resuspended sediments scoured from the upper estuary channel and particularly adjacent wetlands and creeks (De Haas and Eisma, 1993; Wengrove et al., 2015). In the case of the Jiulong estuary, an important component of these areas are mangrove wetlands (Yu et al., 2015). These sediments, deposited during previous periods of low flow, are likely to be rich in labile organic matter when deposited (Yu et al., 2019). Under the extant conditions of relatively high temperatures especially in summer, these sediments act as a biogeochemical incubator undergoing characteristic diagenetic changes (Chen et al., 2018b; Tan et al., 2020; Zhang et al., 2020). As a result of the resuspension of these sediments and their pore waters during the storm, there were considerable changes in the N biogeochemistry of the water column (see following sections). The maximum turbidity was 520 NTU (Rising; Fig. 3c), which was considerably higher than Baseflow values, but less than many previous storms. Thus Yu et al. (2019) found the maximum SPM in the JRE was up to 1500 mg L^{-1} during the peak discharge of 3000 $m^3 s^{-1}$ in 2016. The magnitude of SPM during storms is a result of complex interaction of factors, including the magnitude of the discharge and the period of time since the last major storm (Chen et al.,

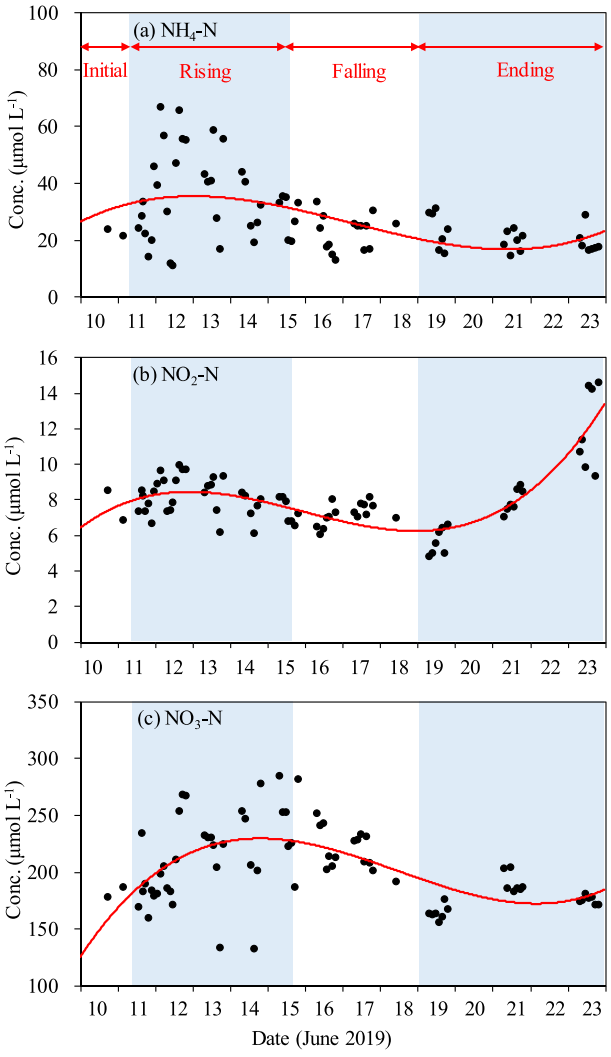

Fig. 6. The intensive measured concentration of (a) ammonium, (b) nitrite and (c) nitrate determined at 0.5 m water depth at Station E in the estuary through the entire sampling period. Red lines are the polynominal fitting curves. (For interpretation of the references to colour in this figure legend, the reader is referred to the web version of this article.)

2018b). It is suggested the relatively low SPM during this storm (June 2019) maybe because this storm was not as intense as some previous storms and because it was the second one of a succession of storms (Fig. 2a) and thus much of the previously deposited sediments had already been flushed out from the upper estuary.

The variation of SPM at Station E was also partially controlled by tide. Throughout the storm, there was higher SPM in the surface water during low tide, because the surface water was carrying higher amounts of river derived SPM (Fig. S1). In addition, there was a significant positive correlation between water velocity and SPM (Fig. S2). The maximum values of landward velocity and SPM were both during the Rising (Table 1). During Baseflow condition, there was relatively higher SPM in ebb tide bringing river derived particles than in flood tide, which contained a higher proportion of particles derived from the brackish part of the estuary. By contrast in the bottom water, there was no difference in the amount of SPM in the water column between ebb and flood tides.

4.2. *Nature of nitrogen discharges into the river during periods of normal flow*

Anthropogenically derived inorganic nitrogen chemical species are discharged into the river and transported towards the estuary (Lin et al., 2020a). Higher fluxes of NH_4-N and NO_2-N were detected in the NJR than WJR during the Baseflow (Fig. 5b, c). Most of the riverine NH_4-N and NO_2-N comes from domestic secondary sewage discharge from Zhangzhou city in the lower reaches of WJR (Chen et al., 2014; Chen et al., 2015) and Longyan City in the upper reaches of NJR (Lin et al., 2020a). An additional important source of these nitrogen compounds is animal wastes, particularly from the intensive pig production in the upper NJR catchment (Cao et al., 2015; Lin et al., 2020a). By contrast NO_3-N predominantly comes from excess ammonium fertilizer added to upstream fields, which is nitrified in or on the soil and then runs off into the river channels. Evidence confirming this pattern comes from the isotopic ratios determined in the water column (Fig. 7) and a recent study by Huang et al. (2020). The slightly lower δ^{15}N-NO_3 in the WJR compared with NJR (Fig. 7a), is inferred to be due to the high fertilizer application in the intensive pomelo orchards in the upper WJR catchment (Lin et al., 2020a). In addition, both manure & sewage (MS) and ammonium fertilizer (AF) can be oxidized by nitrification to nitrate in the oxic water column of the river channels and within surface riverine sediments, particularly during the wet summer season with higher ambient temperature (Lin et al., 2020a). The isotopic content from the Initial to Ending are shown in Fig. 7. The values are consistent with leached soil and groundwater, which resulted in lower δ^{15}N-NO_3 from extensive in-situ nitrification (Fig. 7a, b). Previous work has found that the isotopic values of δ^{15}N-NO_3 and δ^{18}O-NO_3 in both the NJR and WJR during normal flow were the result of nitrate being flushed out into the river from different types of land use (Huang et al., 2020; Lin et al., 2020a). The dominant nitrate source in the NJR was derived from the nitrification of domestic and animal derived sewage (Huang et al., 2020) and as a result had elevated δ^{15}N-NO_3 (+9.2‰ to + 29.7‰, Johannsen et al. (2008)), as shown in Fig. 7a. By contrast in the WJR, most of the nitrate was derived from ammonium fertilizer (Fig. 7b), which was applied to agricultural soil in the watershed and had lower δ^{15}N-NO_3 (0 ± 4‰, Kendall (1998)).

4.3. *Effects of the storm on riverine nitrogen*

As discharge increased during storms, there had an increase in anthropogenic DIN exported from the Jiulong watershed to the estuary (Gao et al., 2018), as has been observed in other river systems (Mooney and McClelland, 2012; Peierls et al., 2003). NH_4-N and NO_2-N increased rapidly in both concentration and total flux (Fig. 4, Fig. 5). A major source of these increased nitrogen compounds was from the flushing of domestic waste from the sewage treatment works of the Zhangzhou City on the WJR (Lin et al., 2020b) together with surface runoff from other agricultural pollutants, such as manure, animal waste and some types of fertilizer from fields in the lower watershed of both WJR and NJR (Chen et al., 2012). Other possible sources are from animal waste particularly in the NJR, though this will take some time before it reaches the estuary (Cao et al., 2015). The negative relationship of δ^{15}N-NH_4 with river discharge in the WJR (Fig. 7d) indicates that dilution by rainfall was the major factor changing the fraction of riverine nitrogen isotope, since the rainwater in South China has a lower δ^{15}N-NH_4 (-12.4‰ to −0.6‰; Jia and Chen (2010)). The only exception was on June 12th (Rising) when there was an increase in isotopic ratio, likely due to ammonia addition of urban sewage with higher δ^{15}N-NH_4 (+9.2‰ to + 29.7‰; Lee et al. (2016)).

By contrast to reduced nitrogen, the increase in concentration of riverine NO_3-N was delayed somewhat with the concentration initially decreasing at the beginning of Rising presumably by rainfall dilution and then increasing to peak value in the later part of Rising (Fig. 4d). This pattern has been observed previous in the Jiulong River (Gao et al., 2018) and in the Elbe River (Jacob et al., 2016). It is likely that this delay is because a major source of NO_3-N is from nitrate present in the surface soil and groundwater, which is leached out as the rainwater infiltrates into the soil and washes the interstitial nitrate out into the stream and

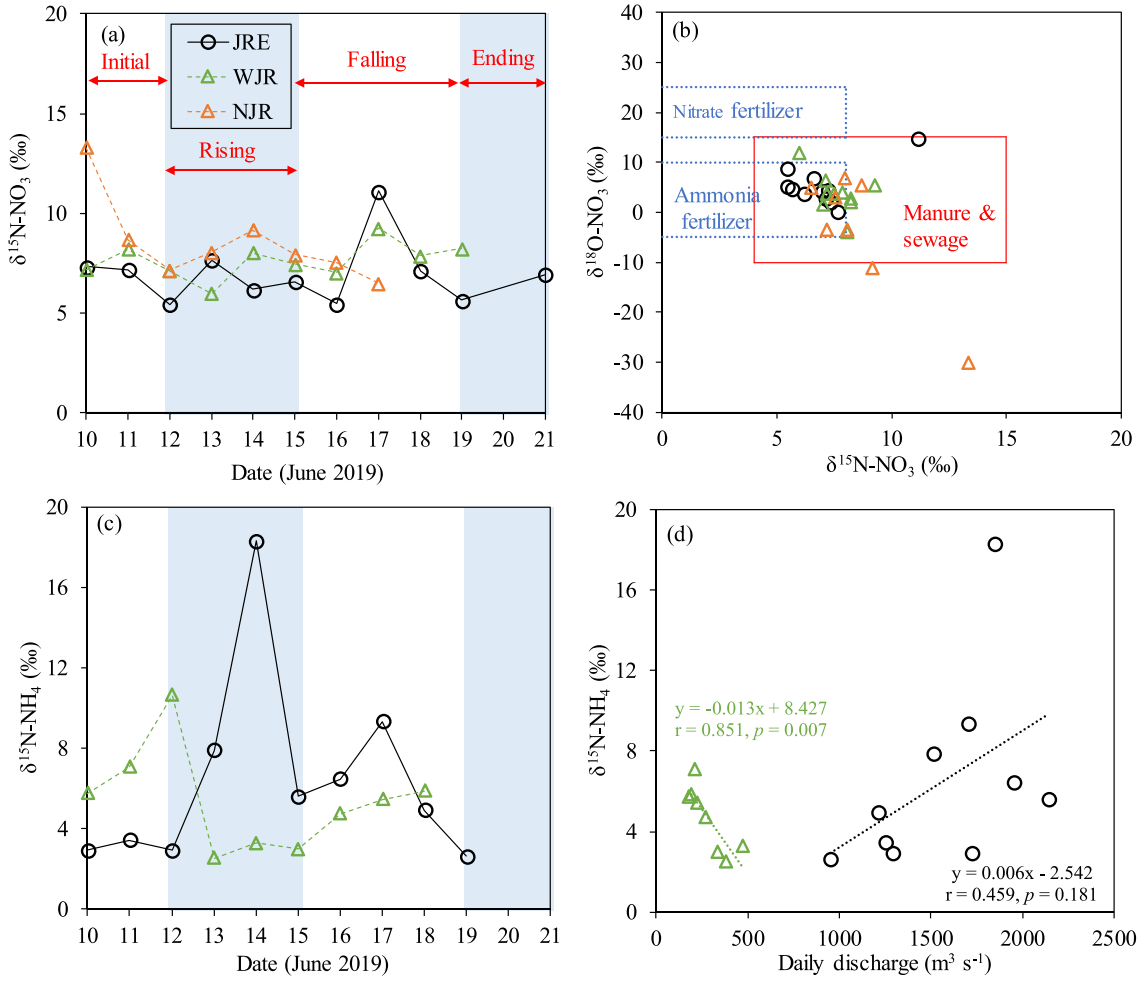

Fig. 7. Distribution of (a) nitrogen isotopic δ^{15}N-NO_3 and (c) δ^{15}N-NH_4 through the sampling period (June 10th to 21st 2019) with the different discharge conditions shown as white/blue shading. The isotopic ratio of δ^{15}N-NH_4 was not measured in the NJR because ammonium concentration was less than the concentration required for isotope determination. (b) shows the distribution of δ^{15}N-NO_3 and δ^{18}O-NO_3 in the rivers (NJR and WJR) and the estuary (JRE). Typical values of possible nitrate sources are shown from Kendall (1998). (d) shows the relationship between δ^{15}N-NH_4 and river daily discharge determined from samples taken daily from both the JRE and WJR. The linear correlations were determined for all samples excluding June 12th for the WJR. (For interpretation of the references to colour in this figure legend, the reader is referred to the web version of this article.)

hence river channels (Johannsen et al., 2008).

4.4. *Effects of the storm on estuarine nitrogen*

In addition to the increase in nitrogen reaching the estuary during the storm as a result of increased river discharge, there was extra inorganic nitrogen added to the estuary water by processes within the tidal river and estuary. This additional concentration and flux was considerably higher during the Rising than other periods (Table 1). This also was the period in which there was major sediment scour from the upper estuary wetlands and catchment runoff. This scour caused the sediment pore waters, which are rich in nitrogen species (dissolved and adsorbed) together with their associated bacteria to be released into the overlying water and observed fluxing past Station E.

In the middle of the Rising, there was a major net increase in NH_4-N which tripled from 24 μmol L^{-1} to a maximum 67 μmol L^{-1} (Fig. 6a), which represented a net increase of greater than 100 t d^{-1} NH_4-N added to the estuary compared to the river flux (Fig. 5a). The anoxic conversion of labile PON to ammonium, is an important process in estuarine sediments, particularly in recent mangrove wetlands, salt marshes and creek sediments adjacent to estuaries (Chen et al., 2018a; Sumi and Koike, 1990). This ammonium is likely to be flushed out by surface sediment scour and catchment runoff in the tidal river during the storm (Fig. S1b). Simultaneously ammonium will be desorbed from resuspended sediment particles, because the concentration of ammonium in the water column of JRE is much lower than that in the surface sediment pore waters (Yu et al., 2020). From its peak of 67 μmol L^{-1} at the beginning of Rising (Fig. 6a), ammonium steadily decreased through the remaining Rising and through Falling to ~ 20 μmol L^{-1}. This decrease in added ammonium could be due to a decrease in the amount of ammonium associated with the scoured estuarine sediments after the first storm pulse (Fig. 2a). However, an additional and likely important contributing factor to this decrease is nitrification in the water column. Evidence for this process comes several observations. Firstly, there was a major increase in nitrate in the water column (see below for discussion of possible other reasons for that increase). In addition, there was increasing gene copies of ammonia-oxidizing microbes with peak values of AOA found in the middle of Rising and AOB in the Falling (Fig. 8a, b). There was also a general decrease in δ^{15}N-NO_3 vs. δ^{18}O-NO_3 through the JRE (except for one anomalous point during the Falling) and a dramatic growth in δ^{15}N-NH_4 (Fig. 7). Such changes are characteristic of nitrification (Böttcher et al., 1990; Casciotti et al., 2002). The observed positive relationship between δ^{15}N-NH_4 and daily river discharge in the JRE (Fig. 7d) suggests that the increased δ^{15}N-NH_4 could derive from nitrification (+14‰ to + 27‰, Casciotti (2009)), though it could also come in part from sewage inputs (+9.2‰ to + 29.7‰, Lee et al. (2016)), as

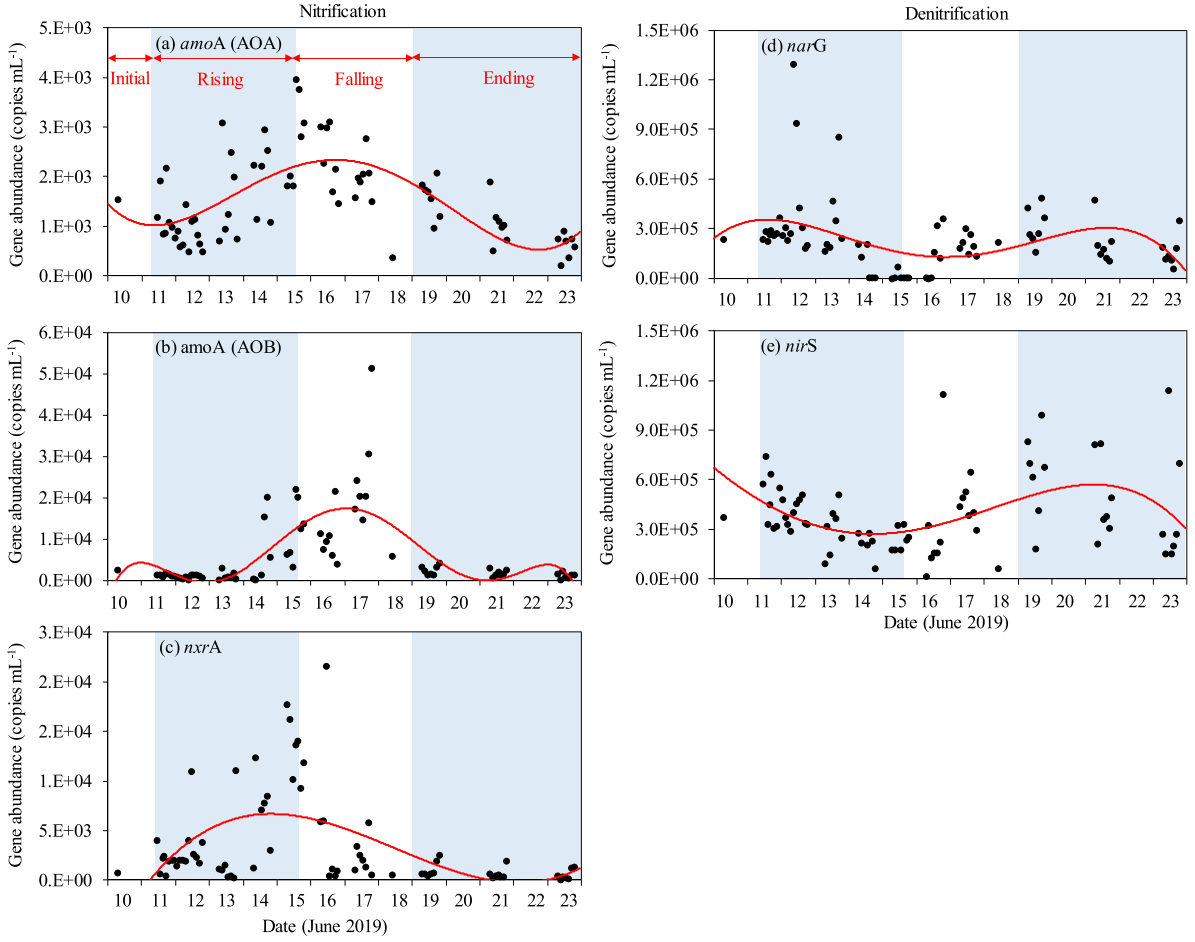

Fig. 8. Distributions of nitrifying (*amo*A and *nxr*A) and denitrifying (*nar*G and *nir*S) gene abundances at Station E through the period of sampling with the different discharge.

shown in Fig. 7c.

The concentration of nitrate between the lower river stations and Station E increased considerably from 175 μmol L^{-1} (Initial) to a maximum of 290 μmol L^{-1} at the end of Rising (Fig. 6c). Part of this increase in nitrate was likely due to nitrification in the water column from ammonium which decreased by 56 μmol L^{-1} from its maximum at the beginning of Rising compared with its concentration at the end of Rising. However, the increase in concentration of nitrate of 115 μmol L^{-1} was much greater than the decrease in ammonium, while the calculated flux of nitrate through the estuary during the Rising was five times more than the flux of ammonium (Table 1). This means that there had to be other sources of nitrate to the estuary other than in-situ nitrification in the water column. There are several possible additional processes which could add nitrate to the estuary during storms. In estuarine and mangrove sediments, there are typically a peak in nitrate at or close to the sediment water interface due to a nitrification–denitrification couple. As surface sediments are resuspended, both nitrate and ammonium will be released into the water column. The relative amounts of nitrate and ammonium will depend on the depth of scoured sediments. It is likely to be particularly rich in nitrate in sediments which are periodically exposed during tidal changes as is typical in mangrove wetlands. An additional contributing factor to this increase in nitrate was a decrease in denitrification. It was observed that there was a decrease in the abundances of denitrifying genes towards the end of Rising, where these genes reached pre-storm abundances only after the Falling (Fig. 8d, e). This is suggestive of a more oxic/less anoxic system in the JRE during the storm. Finally, as noted above for the river sections during storm flow, there was a substantial increase in nitrate which came from ground and soil water discharge, which was slightly delayed from the initial increase in water discharge. It is likely that there was a similar addition of nitrate from the areas in the immediate catchment of the estuary i.e. that the heavy rainfall will cause previously formed nitrate in the adjacent fields and mudflats to be flushed out into the estuary during storm flow. It is not possible without a total nitrate budget to determine the relative importance of these various processes to the observed increase in nitrate through the JRE during the peak of the storm.

During the storm, the concentration of nitrite decreased from the Initial until halfway through the Rising (Fig. 4c), suggesting that nitrite was being diluted by increased discharge more than the increase of nitrite as an intermediate from in-situ nitrification. Nitrite started to increase through the Rising-Falling boundary with the major increase at the end of Ending. During the Baseflow the *amo*A gene (ammonia-oxidizing microbes) was greater than the *nxr*A gene (nitrite oxidation bacteria), while the *nxr*A gene increased substantially during the Flood (Fig. 8a, b, c), when ammonium and the ratio of NH_4-N/DIN had increased in the water column (Table 1). Yan et al. (2019) showed that the ammonium oxidation rate occurred 10–20 times faster than the nitrite oxidation rate during periods of normal flow in the JRE. Thus, nitrite accumulated in normal baseflow condition as a result of incomplete nitrification at the ETM area (Yu et al., 2019). These results suggest there was more complete nitrification during the Flood. Higher denitrifying ratio of *nir*S/*nar*G could also accelerate net nitrite consumption by denitrification (Fig. 8d, e). As the estuary reverted to baseflow during

the Ending, nitrite increased while nitrate decreased in the water column (Fig. 6). This implied that there were non-steady state changes in nitrification and denitrification rates. The sampling was not continued for long enough for the system to revert to its initial steady state condition.

It has been shown, in previous studies of estuaries carried out during normal baseflow, that the wetlands and creeks adjacent to the upper estuary are locations where nutrients are removed and stored (Jickells et al., 2014; Sanders et al., 1997). However, as a result of recent land reclamation in many estuaries, these areas of wetlands have been reduced, thus decreasing the ability of estuaries to act as filters for anthropogenic nutrients fluxing into coastal areas (Jickells et al., 2000; Jickells et al., 2016). In the Jiulong River estuary, the total area of the mangrove wetlands has been considerably reduced over the past 20–30 years (Wang et al., 2018). Despite this reduction of the wetland area, the upper estuary still represents an important location for the removal of anthropogenic nitrogen during normal baseflow (Yu et al., 2019). This area traps sediment containing a high content of labile organic matter (Yu et al., 2015). These surficial sediments then act as a biogeochemical incubator, with diagenetic changes taking place in which labile PON is broken down, ammonia generated, and nitrate formed in the oxic environment found in the surface layers of these tidally affected sediments. It is also a location of considerable dissimilatory and other nitrate reduction (Cao et al., 2016; Zhang et al., 2020). However, in this study, it has been shown that this removal of nutrients is only temporary, since during storms, a large fraction of this anthropogenic nitrogen is remobilised as resuspended sediment which results in an increased pulse of diagenetically altered nitrogen down the estuary to the coastal region. The relative efficiency of the upper estuary as a temporary nutrient filter and biogeochemical incubator depends on various factors including how long the sediment remains in the wetlands and creek, what the ambient temperature was for controlling microbial reaction rate, when and how large the storm is and thus how much of sediment is resuspended.

The results of this study showed the key importance of non-steady state floods in increasing the total flux of DIN exported from the river-estuary systems to the nearby coast. Floods not only result in an increased flux of anthropogenic nitrogen from the river and tidal river catchment but they also remobilize nitrogen which had been temporarily deposited in the estuary during periods of low-normal flow. It is also noted that this storm was a relatively moderate storm in terms of total water discharge. It is likely that storms which occur after a longer period of quiescence and/or storms with higher water discharge, are likely to result in even greater flushing out of pollutant N from the river-estuary system to the coast. This increased DIN flux is likely to result in greater estuarine and coastal eutrophication.

5. Summary

The increased discharge of water from the river during the storm altered the pattern of estuarine salinity, the particle distribution and the location of the ETM. The original location of the ETM during the Baseflow bracketed Station E. However, during the peak of strom flow the freshwater-brackish water boundary moved downstream. The distance downstream was controlled by the strength of storm flow. During the storm in June 2019, the water passing Station E was only freshwater during the high discharge of Rising and then changed back to the tidally changing brackish water characteristic of normal flow conditions as the discharge decreased.

During the storm, the input of SPM brought down the rivers to the estuary increased substantially. In addition, there was also a major increase in sediment added (scoured) in the upper estuary both from the estuary channel and from the adjacent mangrove wetlands and small creeks. As the discharge decreased during the Falling and particularly Ending, both the riverine SPM and added estuarine SPM decreased. Meanwhile, tide also had an effect on the estuarine SPM with higher concentrations during low tide. High water velocity both during high flow periods of ebb and flood tides caused higher SPM.

Both concentrations and fluxes of river inorganic nitrogen increased during the storm. The different land use of the Jiulong River resulted in spatial differences of inorganic nitrogen between the NJR and WJR. The NJR had high ammonium and nitrite from domestic sewage effluent and intensive animal farming in the upper reaches, which were partially oxidized to nitrate by nitrification in the river channel resulting in elevated $\delta^{15}N\text{-}NO_3$. The WJR had higher nitrate from excess ammonium fertilizer in upstream pomelo orchards, resulting in decreased $\delta^{15}N\text{-}NO_3$. In addition, the different sources of inorganic nitrogen also resulted in the different response times of the peak value. Ammonium and nitrite reached peak values at the river mouths faster than nitrate both in the NJR and WJR. The major source of ammonium and nitrite were from domestic waste from the sewage treatment works together with surface runoff from other agricultural pollutants such as manure, animal waste and some types of fertilizer from fields, which caused the peak value of $\delta^{15}N\text{-}NH_4$ in the first day of Rising. However, rainfall decreased $\delta^{15}N\text{-}NH_4$ in most river samples. By contrast, nitrate was delayed somewhat with the concentration firstly decreasing by dilution and then increasing to peak value in the Rising. The major source of nitrate was from leached soil and groundwater, where in-situ nitrification had oxidized ammonium fertilizer.

Apart from the river inputs, the flux of estuarine DIN had increased by 40% ± 8% over the elevated values reaching the estuary during the storm. The additional fluxes of NH_4-N, NO_3-N and NO_2-N were significantly higher in the Rising (55.9 ± 33.4 t d^{-1}, 252.8 ± 59.9 t d^{-1} and 6.2 ± 3.6 t d^{-1}, respectively), particularly for NH_4-N with increased ratio of NH_4-N/DIN. This additional nitrogen mostly came from the scour of surface sediments and catchment runoff in the tidal river, which had been deposited in the upper estuary and adjacent mangrove wetlands and small creeks during periods of normal flow. Following falling discharge, the concentration of NH_4-N decreased both because of decreasing supply from sediment scour after the first storm pulse and due to increased nitrification in the water column. Evidence in support of this was from increased gene copies of nitrifiers (AOA and AOB), which caused a general decrease in $\delta^{15}N\text{-}NO_3$ vs. $\delta^{18}O\text{-}NO_3$ and a dramatic increase in the $\delta^{15}N\text{-}NH_4$. The sources of additional NO_3-N in the estuary came partly from increased nitrification. However, the large increase in NO_3-N flux compared with NH_4-N flux suggested that there were additional processes fluxing nitrate into and through the estuary. One such process was the scouring of surficial mangrove sediments which had a large peak of nitrate in the tidally exposed sediment. Decreased denitrification in the water column was confirmed by the number of copies of the relevant genes (higher *nxr*A and lower *nar*G). An additional major nitrate source came from ground and soil water discharge in the local estuarine catchment, resulting in the delayed peak value as noted above for the river sections.

This study shows the importance of the upper estuary as a temporary location for nitrogen storage in surface sediments, which act as a biogeochemical reactor. At least part of these sediments are resuspended during storms and result in altered nitrogen species being transported into the estuary and from there to the coast.

CRediT authorship contribution statement

Jingjie Lin: Conceptualization, Data curation, Formal analysis, Investigation, Methodology, Project administration, Software. **Michael D. Krom:** Conceptualization, Formal analysis. **Fenfang Wang:** Investigation. **Peng Cheng:** Methodology, Software. **Qibiao Yu:** Methodology, Software. **Nengwang Chen:** Conceptualization, Formal analysis, Funding acquisition, Project administration, Resources.

Declaration of Competing Interest

The authors declare that they have no known competing financial interests or personal relationships that could have appeared to influence

the work reported in this paper.

Acknowledgements

This research was supported by the National Natural Science Foundation of China (No. 41676098; 51961125203). We thank all the students who assisted with fieldwork and Junou Du for technical assistance. This work was completed as we came out of the COVID pandemic, which meant that the collaboration between Xiamen and Haifa was by remote means and not carried out during a visit of Michael D. Krom as originally planned.

Appendix A. Supplementary data

Supplementary data to this article can be found online at https://doi.org/10.1016/j.jhydrol.2022.127438.

References

Annamalai, H., Liu, P., 2005. Response of the Asian summer monsoon to changes in El Niño properties. Q. J. R. Meteorol. Soc. 131 (607), 805–831.
Baborowski, M., von Tümpling, W., Friese, K., 2004. Behaviour of suspended particulate matter (SPM) and selected trace metals during the 2002 summer flood in the River Elbe (Germany) at Magdeburg monitoring station. Hydrol. Earth Syst. Sci. 8 (2), 135–150.
Bai, Z., Zhao, J., Wei, Z., Jin, X., Ma, L., 2019. Socio-economic drivers of pig production and their effects on achieving sustainable development goals in China. J. Integr. Environ. Sci. 16 (1), 141–155.
Böttcher, J., Strebel, O., Voerkelius, S., Schmidt, H.-L., 1990. Using isotope fractionation of nitrate nitrogen and nitrate oxygen for evaluation of microbial denitrification in a sandy aquifer. J. Hydrol. 114 (3-4), 413–424.
Canfield, D.E., Glazer, A.N., Falkowski, P.G., 2010. The evolution and future of earth's nitrogen cycle. Science 330 (6001), 192–196.
Cao, W., Hong, H., Yue, S., 2005. Modelling agricultural nitrogen contributions to the Jiulong River estuary and coastal water. Global Planet. Change 47 (2-4), 111–121.
Cao, W., Huang, Z., Zhai, W., Li, Y., Hong, H., 2015. Isotopic evidence on multiple sources of nitrogen in the northern Jiulong River, Southeast China. Estuar. Coast. Shelf Sci. 163, 37–43.
Cao, W., Yang, J., Li, Y., Liu, B., Wang, F., Chang, C., 2016. Dissimilatory nitrate reduction to ammonium conserves nitrogen in anthropogenically affected subtropical mangrove sediments in Southeast China. Mar. Pollut. Bull. 110 (1), 155–161.
Casciotti, K.L., 2009. Inverse kinetic isotope fractionation during bacterial nitrite oxidation. Geochim. Cosmochim. Acta 73 (7), 2061–2076.
Casciotti, K.L., Sigman, D.M., Hastings, M.G., Böhlke, J.K., Hilkert, A., 2002. Measurement of the oxygen isotopic composition of nitrate in seawater and freshwater using the denitrifier method. Anal. Chem. 74 (19), 4905–4912.
Chen, N., Wu, J., Chen, Z., Lu, T., Wang, L., 2014. Spatial-temporal variation of dissolved N2 and denitrification in an agricultural river network, southeast China. Agric. Ecosyst. Environ. 189, 1–10.
Chen, N., Krom, M.D., Wu, Y., Yu, D., Hong, H., 2018a. Storm induced estuarine turbidity maxima and controls on nutrient fluxes across river-estuary-coast continuum. Sci. Total Environ. 628-629, 1108–1120.
Chen, N., Wu, J., Zhou, X., Chen, Z., Lu, T., 2015. Riverine N_2O production, emissions and export from a region dominated by agriculture in Southeast Asia (Jiulong River). Agric. Ecosyst. Environ. 208, 37–47.
Chen, N., Wu, J., Hong, H., 2012. Effect of storm events on riverine nitrogen dynamics in a subtropical watershed, southeastern China. Sci. Total Environ. 431, 357–365.
Chen, Y., Chen, N., Li, Y., Hong, H., 2018b. Multi-timescale sediment responses across a human impacted river-estuary system. J. Hydrol. 560, 160–172.
Cheng, P., Mao, J., Yu, F., Chen, N., Wang, A., Xu, F., 2019. A numerical study of residual flow induced by eddy viscosity-shear covariance in a tidally energetic estuary. Estuar. Coast. Shelf Sci. 230, 13–26.
Cheng, P., Yu, F., Chen, N., Wang, A., 2020. Observational study of tidal mixing asymmetry and eddy viscosity-shear covariance – induced residual flow in the Jiulong River estuary. Cont. Shelf Res. 193, 104035–104044.
De Girolamo, A.M., D'Ambrosio, E., Pappagallo, G., Rulli, M.C., Lo Porto, A., 2017. Nitrate concentrations and source identification in a Mediterranean river system. Rendiconti Lincei-Scienze Fisiche E Naturali 28 (2), 291–301.
De Haas, H., Eisma, D., 1993. Suspended-sediment transport in the Dollard estuary. Neth. J. Sea Res. 31 (1), 37–42.
Dong, L.F., Smith, C.J., Papaspyrou, S., Stott, A., Osborn, A.M., Nedwell, D.B., 2009. Changes in benthic denitrification, nitrate ammonification, and anammox process rates and nitrate and nitrite reductase gene abundances along an estuarine nutrient gradient (the Colne estuary, United Kingdom). Appl. Environ. Microbiol. 75 (10), 3171–3179.
Duce, R.A., LaRoche, J., Altieri, K., Arrigo, K.R., Baker, A.R., Capone, D.G., Cornell, S., Dentener, F., Galloway, J., Ganeshram, R.S., Geider, R.J., Jickells, T., Kuypers, M.M., Langlois, R., Liss, P.S., Liu, S.M., Middelburg, J.J., Moore, C.M., Nickovic, S., Oschlies, A., Pedersen, T., Prospero, J., Schlitzer, R., Seitzinger, S., Sorensen, L.L., Uematsu, M., Ulloa, O., Voss, M., Ward, B., Zamora, L., 2008. Impacts of atmospheric anthropogenic nitrogen on the open ocean. Science 320 (5878), 893–897.
Francis, C.A., Roberts, K.J., Beman, J.M., Santoro, A.E., Oakley, B.B., 2005. Ubiquity and diversity of ammonia-oxidizing archaea in water columns and sediments of the ocean. PNAS 102 (41), 14683–14688.
Galloway, J., Dentener, F., Capone, D., Boyer, E., Howarth, R., 2004. Nitrogen cycles: past, present, and future. Biogeochemistry, 70(2): 153–226.
Galloway, J.N., Townsend, A.R., Erisman, J.W., Bekunda, M., Cai, Z., Freney, J.R., Martinelli, L.A., Seitzinger, S.P., Sutton, M.A., 2008. Transformation of the nitrogen cycle: recent trends, questions, and potential solutions. Science 320 (5878), 889–892.
Gao, X., Chen, N., Yu, D., Wu, Y., Huang, B., 2018. Hydrological controls on nitrogen (ammonium versus nitrate) fluxes from river to coast in a subtropical region: Observation and modeling. J. Environ. Manage. 213, 382–391.
Holmes, R., McClelland, J., Sigman, D., Fry, B., Peterson, B., 1998. Measuring N^{15}-NH_4^+ in marine, estuarine and fresh waters: An adaptation of the ammonia diffusion method for samples with low ammonium concentrations. Mar. Chem. 60 (3–4), 235–243.
Huang, Y., Huang, J., Ervinia, A., Duan, S., 2020. Tracking riverine nitrate sources under changing land use pattern and hydrologic regime. Mar. Pollut. Bull. 152, 10–19.
Jacob, J., Sanders, T., Daehnke, K., 2016. Nitrite consumption and associated isotope changes during a river flood event. Biogeosciences 13 (19), 5649–5659.
Jia, G., Chen, F., 2010. Monthly variations in nitrogen isotopes of ammonium and nitrate in wet deposition at Guangzhou, south China. Atmos. Environ. 44 (19), 2309–2315.
Jickells, T., Andrews, J., Samways, G., Sanders, R., Malcolm, S., Sivyer, D., Parker, R., Nedwell, D., Trimmer, M., Ridgway, J., 2000. Nutrient fluxes through the Humber estuary – past, present and future. Ambio 29 (3), 130–135.
Jickells, T.D., Andrews, J.E., Parkes, D.J., 2016. Direct and indirect effects of estuarine reclamation on nutrient and metal fluxes in the global coastal zone. Aquat. Geochem. 22 (4), 337–348.
Jickells, T.D., Andrews, J.E., Parkes, D.J., Suratman, S., Aziz, A.A., Hee, Y.Y., 2014. Nutrient transport through estuaries: The importance of the estuarine geography. Estuar. Coast. Shelf Sci. 150, 215–229.
Johannsen, A., Dähnke, K., Emeis, K., 2008. Isotopic composition of nitrate in five German rivers discharging into the North Sea. Org Geochem. 39 (12), 1678–1689.
Jung, J., Yeom, J., Kim, J., Han, J., Lim, H.S., Park, H., Hyun, S., Park, W., 2011. Change in gene abundance in the nitrogen biogeochemical cycle with temperature and nitrogen addition in Antarctic soils. Res. Microbiol. 162 (10), 1018–1026.
Kaiser, D., Unger, D., Qiu, G., 2014. Particulate organic matter dynamics in coastal systems of the northern Beibu gulf. Cont. Shelf Res. 82, 99–118.
Kaushal, R., Lai, C., Shiah, F., Liang, M., 2021. Utilization of Delta $\Delta^{17}O$ for nitrate dynamics in a subtropical freshwater reservoir. Sci. Total Environ. 753, 141836–141846.
Kendall, C., 1998. Tracing nitrogen sources and cycling in catchments. In: Kendall, C., McDonnell, J.J. (Eds.), Isotope Tracers in Catchment Hydrology. Elsevier, Amsterdam, pp. 519–576.
Kessler, A.J., Roberts, K.L., Bissett, A., Cook, P.L.M., 2018. Biogeochemical controls on the relative importance of denitrification and dissimilatory nitrate reduction to ammonium in estuaries. Global Biogeochem. Cycles 32 (7), 1045–1057.
Koschorreck, M., Darwich, A., 2003. Nitrogen dynamics in seasonally flooded soils in the Amazon floodplain. Wetlands Ecol. Manage. 11 (5), 317–330.
Lee, J., Park, T., Kim, M.-S., Kim, J., Lee, S., Lee, S.K., Lee, Y.S., Lee, W.-S., Yu, S., Rhew, D., 2016. Stable isotope on the evaluation of water quality in the presence of WWTPs in rivers. Environ. Sci. Pollut. Res. 23 (18), 18175–18182.
Lin, J., Chen, N., Yuan, X., Tian, Q., Hu, A., Zheng, Y.i., 2020a. Impacts of human disturbance on the biogeochemical nitrogen cycle in a subtropical river system revealed by nitrifier and denitrifier genes. Sci. Total Environ. 746, 141150.
Lin, J., Chen, N., Wang, F., Huang, Z., Zhang, X., Liu, L., 2020b. Urbanization increased river nitrogen export to western Taiwan Strait despite increased retention by nitrification and denitrification. Ecol. Ind. 109, 105756–105765.
Liu, G.D., Wu, W.L., Zhang, J., 2005. Regional differentiation of non-point source pollution of agriculture-derived nitrate nitrogen in groundwater in northern China. Agric. Ecosyst. Environ. 107 (2-3), 211–220.
López-Gutiérrez, J.C., Henry, S., Hallet, S., Martin-Laurent, F., Catroux, G., Philippot, L., 2004. Quantification of a novel group of nitrate-reducing bacteria in the environment by real-time PCR. J. Microbiol. Methods 57 (3), 399–407.
Marcé, R., Schiller, D., Aguilera, R., Martí, E., Bernal, S., 2018. Contribution of hydrologic opportunity and biogeochemical reactivity to the variability of nutrient retention in river networks. Global Biogeochem. Cycles 32 (3), 376–388.
Mooney, R.F., McClelland, J.W., 2012. Watershed export events and ecosystem responses in the Mission-Aransas national estuarine research reserve, South Texas. Estuaries Coasts 35 (6), 1468–1485.
Oczkowski AJ, Santos EA, Martin RM, Gray AB, Hanson AR, Watson EB, Huertas E, Wigand C. 2020. Unexpected nitrogen sources in a tropical urban estuary. J. Geophys. Res.: Biogeosciences, 125(3): e2019JG005502.
Peierls, B.L., Christian, R.R., Paerl, H.W., 2003. Water quality and phytoplankton as indicators of hurricane impacts on a large estuarine ecosystem. Estuaries 26 (5), 1329–1343.
Rotthauwe, J.H., Witzel, K.P., Liesack, W., 1997. The ammonia monooxygenase structural gene amoA as a functional marker: Molecular fine-scale analysis of natural ammonia-oxidizing populations. Appl. Environ. Microl. 63 (12), 4704–4712.
Rozemeijer, J., Noordhuis, R., Ouwerkerk, K., Dionisio Pires, M., Blauw, A., Hooijboer, A., van Oldenborgh, G.J., 2021. Climate variability effects on eutrophication of groundwater, lakes, rivers, and coastal waters in the Netherlands. Sci. Total Environ. 771, 145380.

Sanders, R.J., Jickells, T., Malcolm, S., Brown, J., Kirkwood, D., Reeve, A., Taylor, J., Horrobin, T., Ashcroft, C., 1997. Nutrient fluxes through the Humber estuary. J. Sea Res. 37 (1-2), 3–23.
Sigman, D.M., Casciotti, K.L., Andreani, M., Barford, C., Galanter, M., Böhlke, J.K., 2001. A bacterial method for the nitrogen isotopic analysis of nitrate in seawater and freshwater. Anal. Chem. 73 (17), 4145–4153.
Smith, C., Dong, L., Wilson, J., Stott, A., Osborn, A., 2015. Seasonal variation in denitrification and dissimilatory nitrate reduction to ammonia process rates and corresponding key functional genes along an estuarine nitrate gradient. Front. Microbiol. 6, 542–552.
Sumi, T., Koike, I., 1990. Estimation of ammonification and ammonium assimilation in surficial coastal and estuarine sediment. Limnol. Oceanogr. 35 (2), 270–286.
Tan, E., Zou, W., Zheng, Z., Yan, X., Du, M., Hsu, T.-C., Tian, L.i., Middelburg, J.J., Trull, T.W., Kao, S.-j., 2020. Warming stimulates sediment denitrification at the expense of anaerobic ammonium oxidation. Nat. Clim. Change 10 (4), 349–355.
Tilman, D., Cassman, K.G., Matson, P.A., Naylor, R., Polasky, S., 2002. Agricultural sustainability and intensive production practices. Nature 418 (6898), 671–677.
Vitousek, P.M., Aber, J.D., Howarth, R.W., Likens, G.E., Matson, P.A., Schindler, D.W., Schlesinger, W.H., Tilman, D.G., 1997. Human alteration of the global nitrogen cycle: sources and consequences. Ecol. Appl. 7 (3), 737–750.
Wang, F., Chen, N., Yan, J., Lin, J., Guo, W., Cheng, P., Liu, Q., Huang, B., Tian, Y., 2019. Major processes shaping mangroves as inorganic nitrogen sources or sinks: insights from a multidisciplinary study. J. Geophys. Res.-Biogeosci. 124 (5), 1194–1208.
Wang, F., Cheng, P., Chen, N., Kuo, Y., 2021. Tidal driven nutrient exchange between mangroves and estuary reveals a dynamic source-sink pattern. Chemosphere 270, 128665–128674.
Wang, M., Cao, W., Guan, Q., Wu, G., Wang, F., 2018. Assessing changes of mangrove forest in a coastal region of southeast China using multi-temporal satellite images. Estuar. Coast. Shelf Sci. 207, 283–292.
Wengrove, M.E., Foster, D.L., Kalnejais, L.H., Percuoco, V., Lippmann, T.C., 2015. Field and laboratory observations of bed stress and associated nutrient release in a tidal estuary. Estuar. Coast. Shelf Sci. 161, 11–24.
Wertz, S., Poly, F., Le Roux, X., Degrange, E., 2008. Development and application of a PCR-denaturing gradient gel electrophoresis tool to study the diversity of Nitrobacter-like nxrA sequences in soil. FEMS Microbiol. Ecol. 63 (2), 261–271.
Whitehead, P.G., Sarkar, S., Jin, L., Futter, M.N., Caesar, J., Barbour, E., Butterfield, D., Sinha, R., Nicholls, R., Hutton, C., Leckie, H.D., 2015. Dynamic modeling of the Ganga river system: impacts of future climate and socio-economic change on flows and nitrogen fluxes in India and Bangladesh. Environ. Sci.-Processes Impacts 17 (6), 1082–1097.
Yan, X., Wan, X.S., Liu, L.i., Xu, M.N., Tan, E., Zheng, Z., Zou, W., Tian, L.i., Li, D.-W., Trull, T.W., Kao, S.-J., 2019. Biogeochemical dynamics in a eutrophic tidal estuary revealed by isotopic compositions of multiple nitrogen species. J. Geophys. Res.-Biogeosciences 124 (7), 1849–1864.
Yu, D., Chen, N., Cheng, P., Yu, F., Hong, H., 2020. Hydrodynamic impacts on tidal-scale dissolved inorganic nitrogen cycling and export across the estuarine turbidity maxima to coast. Biogeochemistry 151 (1), 81–98.
Yu, D., Chen, N., Krom, M.D., Lin, J., Cheng, P., Yu, F., Guo, W., Hong, H., Gao, X., 2019. Understanding how estuarine hydrology controls ammonium and other inorganic nitrogen concentrations and fluxes through the subtropical Jiulong River Estuary, SE China under baseflow and flood-affected conditions. Biogeochemistry 142 (3), 443–466.
Yu, X., Yang, J., Liu, L., Tian, Y., Yu, Z., 2015. Effects of Spartina alterniflora invasion on biogenic elements in a subtropical coastal mangrove wetland. Environ. Sci. Pollut. Res. 22 (4), 3107–3115.
Zhang, M., Dai, P., Lin, X., Lin, L., Hetharua, B., Zhang, Y., Tian, Y., 2020. Nitrogen loss by anaerobic ammonium oxidation in a mangrove wetland of the Zhangjiang Estuary, China. Sci. Total Environ. 698, 134291.
Zhang, X., Zhang, Y., Shi, P., Bi, Z., Shan, Z., Ren, L., 2021. The deep challenge of nitrate pollution in river water of China. Sci. Total Environ. 770, 144674–144685.